Journal of Colloid and Interface Science 579 (2020) 707–713

Contents lists available at ScienceDirect

Journal of Colloid and Interface Science

journal homepage: www.elsevier.com/locate/jcis

Interface engineering in CeO_2 (1 1 1) facets decorated with CdSe quantum dots for photocatalytic hydrogen evolution

Yongjin Ma [a,1], Pengfei Ou [b,1], Ziyu Wang [c,*], Anquan Zhu [a], Lili Lu [a], Yuhui Zhang [a], Weixuan Zeng [a], Jun Song [b,*], Jun Pan [a,*]

[a] State Key Laboratory for Powder Metallurgy, Central South University, Changsha Lushan South Road 932, 410083, China
[b] Department of Mining and Materials Engineering, McGill University, Montreal, Quebec H3A 0C5, Canada
[c] The Institute of Technological Sciences, Wuhan University, Wuhan Bayi Road 299, 430072, China

GRAPHICAL ABSTRACT

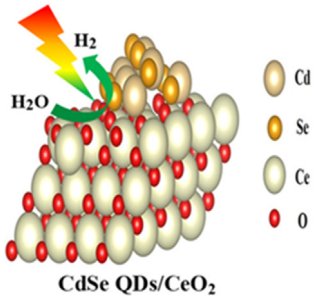

ARTICLE INFO

Article history:
Received 3 May 2020
Revised 22 June 2020
Accepted 23 June 2020
Available online 27 June 2020

Keywords:
H_2 evolution reaction
CdSe QDs
CdSe QDs/CeO_2(1 1 1) heterostructures
Density functional theory

ABSTRACT

The interfaces of heterostructures have been widely studied in the field of photocatalytic H_2 evolution reaction (HER). In the present study, the CdSe QDs/CeO_2(1 1 1) heterostructures were synthesized by wet chemistry method. The CdSe QDs/CeO_2(1 1 1)-0.075 showed higher photocatalytic H_2 evolution with 283.32 μmol $g^{-1}h^{-1}$, because of the enhanced light absorbance intensity and edge, lower recombination, higher separation and transfer, as well as longer lifetime of the photogenerated carrier. Density functional theory (DFT) calculations further confirmed that the enhanced HER activity of CdSe QDs/CeO_2(1 1 1) heterostructures is resulted from a stronger water adsorption, a lower energy barrier of water dissociation and a more optimal free energy of hydrogen adsorption than CdSe and CeO_2. The strategy of construction heterostructures provides a promising pathway for enhancing the performance of photocatalytic H_2 evolution as well as other catalytic reactions.

1. Introduction

The H_2, synthesized by water splitting reaction ($2H_2O \rightarrow 2H_2 + O_2$), is crucial clean energy in the practical fuel cells and other industrial applications owed to its high energy density and energy conversion efficiency. [1–6] For decades, the importance of the metal oxides with remarkable redox properties, such as ceria (CeO_2), titanium oxide (TiO_2), and zinc oxide (ZnO), has been studied widely for the water splitting. [7–11] CeO_2 has attracted enormous attention due to its low cost, stability, and superior catalytic properties. [12–15] It has been suggested that the photocatalytic activity of CeO_2 are strongly dependent on its surface morphology due to the different chemical and electronic

* Corresponding authors.
E-mail addresses: zywang@whu.edu.cn (Z. Wang), jun.song2@mcgill.ca (J. Song), jun.pan@csu.edu.cn (J. Pan).
[1] These authors contributed equally to this work.

https://doi.org/10.1016/j.jcis.2020.06.100
0021-9797/

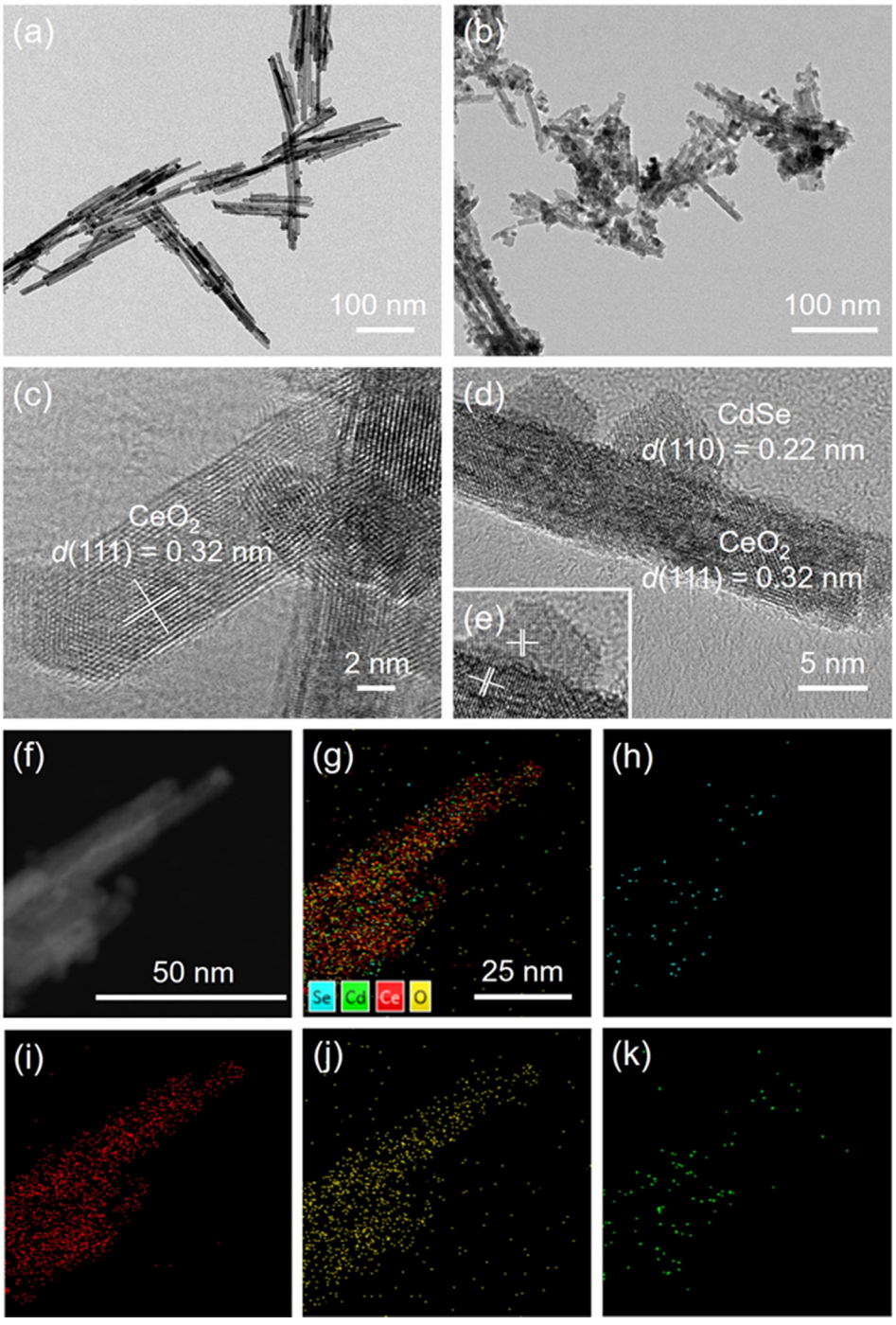

Fig. 1. The TEM images of (a) Pure CeO_2 and (b) CdSe QDs/CeO_2-0.075; the HRTEM images of (c) Pure CeO_2 and (d) CdSe QDs/CeO_2-0.075; (e) the interface of CdSe QDs and CeO_2. The TEM-EDS elemental mapping images for (f) CdSe QDs/CeO_2-0.075; (g) the mapping image of all elements; (h) Cd; (i) Ce; (j) O; (k) Se.

properties from different surface facets. Various methods have been developed to tune the facets on the surface of CeO_2 by controlling its morphologies, e.g., through the means of nanocubes, octahedrons and nanorods. [16–18] The (111), (110) and (100) surface facets of CeO_2 are three most common. Within them, the (111) surface facets of CeO_2 consists of Ce and O atoms in a single plane while the (110) and (100) facets are corrugated, exposing either Ce or O atoms on the surfaces. [19–20] Based on the previous study, (111) facet is suggested to be more stable than (110) and (100) facets. [21] In addition, it has been proposed that the (111) facet facilitates the H_2 evolution reaction and is responsible for the outstanding performance of CeO_2 nanorods. [22]

However, CeO_2 has unfavorable drawbacks including wide band gap ($E_g(CeO_2)$ = 2.92 eV) and recombination of photogenerated carrier, which lead to lower photocatalytic efficiency. [23–24] Therefore, constructing the heterostructure improves the visible-light response, reduces the recombination of photogenerated carrier and promotes the transfer and separation of charges. [25–28] CdSe QDs exhibit wide visible-light response, and have been extensively studied in the photocatalytic field. [29–33] With the exposed (111) facets of the CeO_2 nanorods, a deeper understanding can be gained about the interaction of specific surface facets with and their impact on photocatalytic activity.

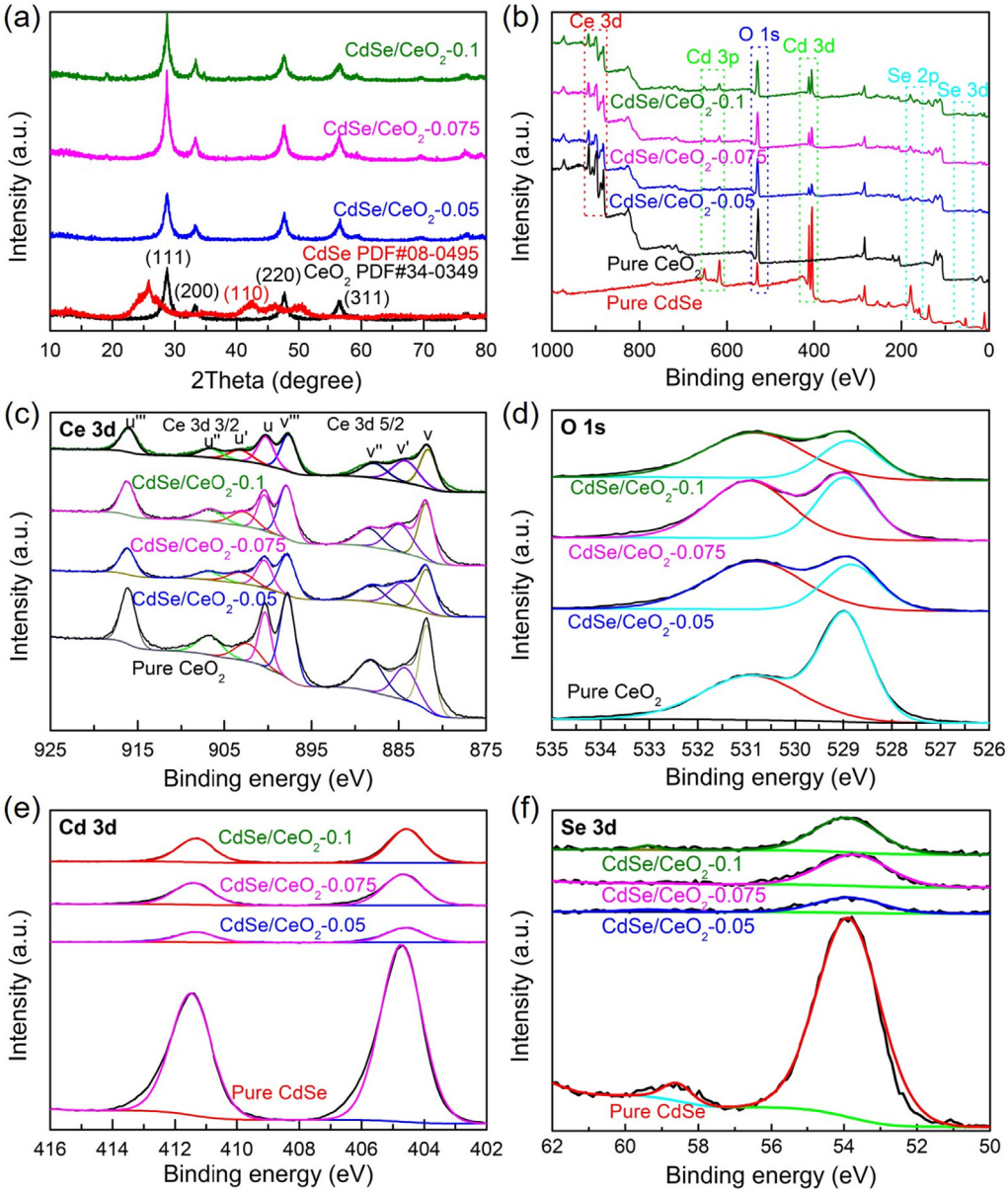

Fig. 2. (a) the XRD patterns of as-obtained samples. The XPS patterns of as-obtained samples for (b) the survey spectra; (c) Ce 3d; (d) O1s; (e) Cd 3d; (f) Se 3d.

The fundamental photocatalytic H_2 evolution process is believed to consist of three steps: (1) the carrier generated on semiconductors under light irradiation; (2) the separation and transfer of photogenerated charges; (3) The reacting species (H_2O/OH^-, H_2O/H^+) generated on the surfaces. Herein, we take advantage of the wet chemistry method to create CdSe QDs/CeO_2 heterostructures for the photocatalytic H_2 evolution reaction. We performed electrochemical impedance spectroscopy (EIS), photoluminescence (PL) and transient photoluminescence (TRPL) to explore the separation and transfer of photogenerated carriers on the interface. Consequently, the synergetic effect of CdSe could be beneficial to the visible-light absorption and charge separation abilities of CdSe QDs/CeO_2 composites, resulting in high photocatalytic H_2 evolution performance. Moreover, density functional theory (DFT) calculations were also carried out to further elucidate the intrinsic role of the interface in the CdSe QDs/CeO_2(111) heterostructures on photocatalytic H_2 evolution reaction.

2. Results and discussion

By comparing the transmission electron microscope (TEM) images in Fig. 1 (a-e), it is clear that CdSe QDs loaded on the CeO_2 (111) for CdSe QDs/CeO_2-0.075. The HRTEM images of pure CeO_2 and CdSe QDs/CeO_2-0.075 were shown in Fig. 1 (c) and (d), respectively. From the images, the planar distance of 0.32 nm corresponds to the spacing between adjacent (111) planes of CeO_2 nanorods, while the 0.22 nm spacing is associated with the (110) planes of CdSe, as shown in the Fig. 1 (d) and (e). Additionally, TEM-EDS was carried out to display the elemental distribution of the CdSe QDs/CeO_2-0.075 as shown in Fig. 1 (f)-(k). The Ce, O, Cd and Se distributed uniformly in the CdSe QDs/CeO_2 nanorods, which further indicated that the CdSe QDs are distributed on the CeO_2 surface. The nanostructure of CdSe QDs-decorated CeO_2 with exposed (111) facets was synthesized by the wet chemistry method. The morphology images were showed in Fig. S1 in the Supporting Information.

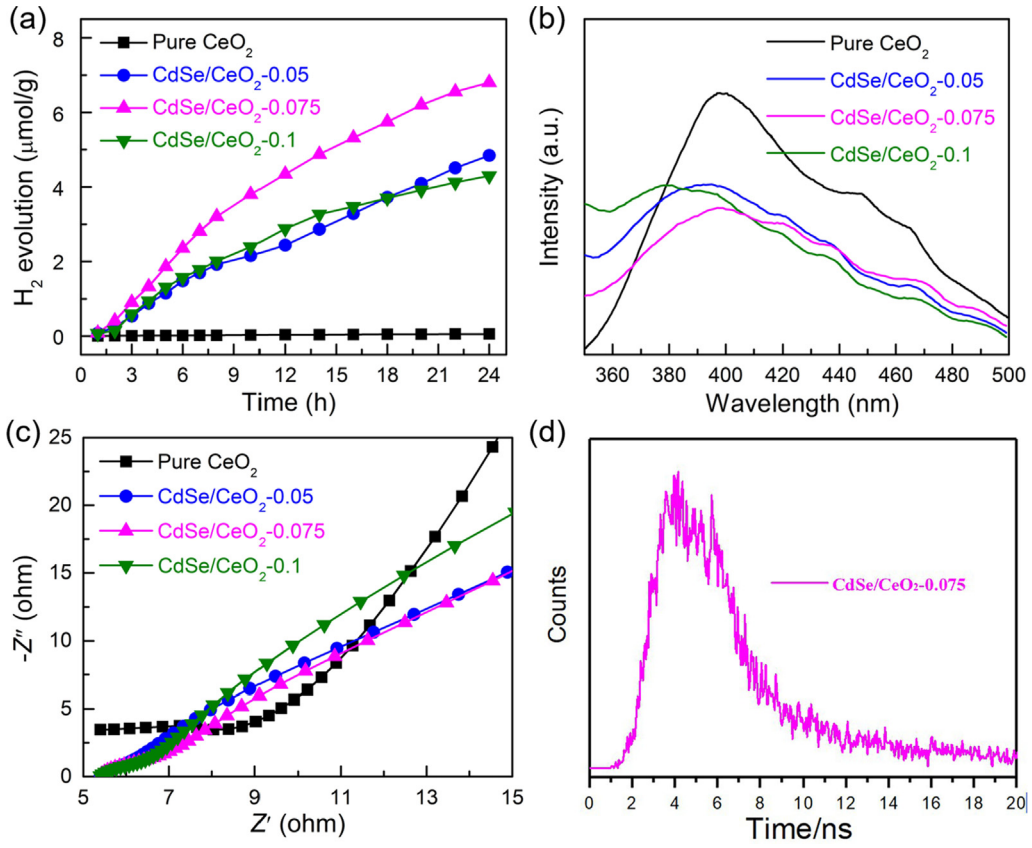

Fig. 3. (a) Photocatalytic hydrogen evolution in 24 h; (b) The PL plot; (c) The EIS plots of the as-obtained samples; (d) the TRPL plot of the as-obtained samples.

The crystallographic structures of the as-obtained samples were examined as shown in Fig. 2 (a) by X-ray diffraction (XRD). For pure CeO_2, the major reflections peaks at 2θ values of 28.53°, 33.01°, 47.44° and 56.34° can be observed, which macth well with the (111), (200), (220) and (311) planes of the CeO_2 crystal (PDF # 34–0349). In the XRD pattern of pure CdSe, the major reflections peaks at 2θ values of 23.90°, 25.35°, 27.08°, 41.97° and 45.79° can be observed, which match well with the (100), (002), (101), (110) and (103) planes of the CdSe crystal (PDF # 08–0495).With respect to the CdSe QDs/ CeO_2 samples, the typical diffraction peaks of CeO_2 and (110) of CdSe QDs can be clearly observed. In comparison with pure CeO_2, no remarkable difference can be observed for the CdSe QDs/CeO_2 samples. Some peaks of CdSe are weak and not apparent due to its low content. The atomic concentrations and chemical states of surface components of CeO_2, CdSe and CdSe QDs/CeO_2 samples were investigated by X-ray photoelectron spectroscopy (XPS). The XPS survey spectra displayed that the CeO_2 and CdSe contains the elements of Ce, O, Cd, and Se, respectively; Ce, O, Cd, and Se can be observed in the XPS survey spectrum of CdSe QDs/CeO_2 composites, which implied CeO_2 and CdSe coexist in the CdSe QDs/CeO_2 composites as shown in Fig. 2 (b). Eight peaks of Ce 3d can be observed (Fig. 2 (c)), with the peaks at 881.62 eV (v), 884.41 eV (v'), 887.97 eV (v''), and 897.65 eV (v''') are assigned to Ce $3d_{5/2}$, and the peaks at 900.39 eV (u), 903.38 eV (u'), 906.66 eV (u''), and 916.16 eV (u''') are ascribed to Ce $3d_{3/2}$. Based on previous literatures, the v, v'', v''', and u' are corresponding to the Ce^{3+} chemical valence, and the v', u, u'', and u''' are corresponding to the main Ce^{4+} chemical valence in the hybrids. Meanwhile, two peaks can be observed in the O 1 s spectrum as shown in Fig. 2 (d). The peak at 529.00 eV is indexed to the Ce-O and the other peak at 530.95 eV is related to adsorbed oxygen and H_2O. Interestingly, the Ce-O peaks of CdSe QDs/CeO_2 composites moved to lower binding energy, which indicated that CdSe QDs can enhance stability of Ce-O. Besides, the Cd 3d and Se 3d peaks are shown in Fig. 2 (e) and (f). The intensity of Ce 3d peaks of CdSe QDs/CeO_2 composites are decreased compared to that of pure CeO_2 due to the reduced amount of pure CeO_2, the intensity of Cd and Se peaks are increased with the increased amount of CdSe for CdSe QDs/CeO_2 composites. The above results demonstrate that the CdSe QDs/ CeO_2 composites are obtained, and the chemical valences of elements are clearly distinguished.

The photocatalytic hydrogen evolution performance of the as-obtained photocatalysts was evaluated under visible-light. CdSe QDs/CeO_2 composites display enhanced photocatalytic HER performance compared to pure CeO_2, as shown in Fig. 3 (a). The average rate of pure CeO_2, CdSe QDs/CeO_2-0.05, CdSe QDs/CeO_2-0.075 and CdSe QDs/CeO_2-0.1 are 2.25, 201.88, 283.32 and 178.8 μmol $g^{-1}h^{-1}$ respectively, as shown in Fig. S2 in the Supporting Information. Both S^{2-} and SO_3^{2-} were regarded as sacrificial agent in the system. The S^{2-} was possibly doped into CdSe, so that XPS results of samples after reactions was performed to exclude the S doping in Fig. S3 and Table S1 in the Supporting Information. The PL spectra is shown in Fig. 3 (b), which can reflect the separation efficiency of photogenerated charges. It can be found that the spectra intensity of CdSe QDs/CeO_2 composites exhibit a remarkable reduction compared to that of pure CeO_2. Interestingly, with respect to the CdSe QDs/CeO_2-0.05 and CdSe QDs/CeO_2-0.1, the CdSe QDs/CeO_2-0.075 exhibits obviously lower intensity, demonstrating that CdSe QDs/ CeO_2 composites can decrease the recombination of photogenerated carriers. Furthermore, the EIS plot was performed to investigate the separation efficiency of photogenerated charge carriers as shown in Fig. 3 (c). Interestingly, CdSe/CeO_2 composites illustrate improved transfer of photogenerated charge carriers and thus boost the photocatalytic efficiency. Simultaneously, the photogen-

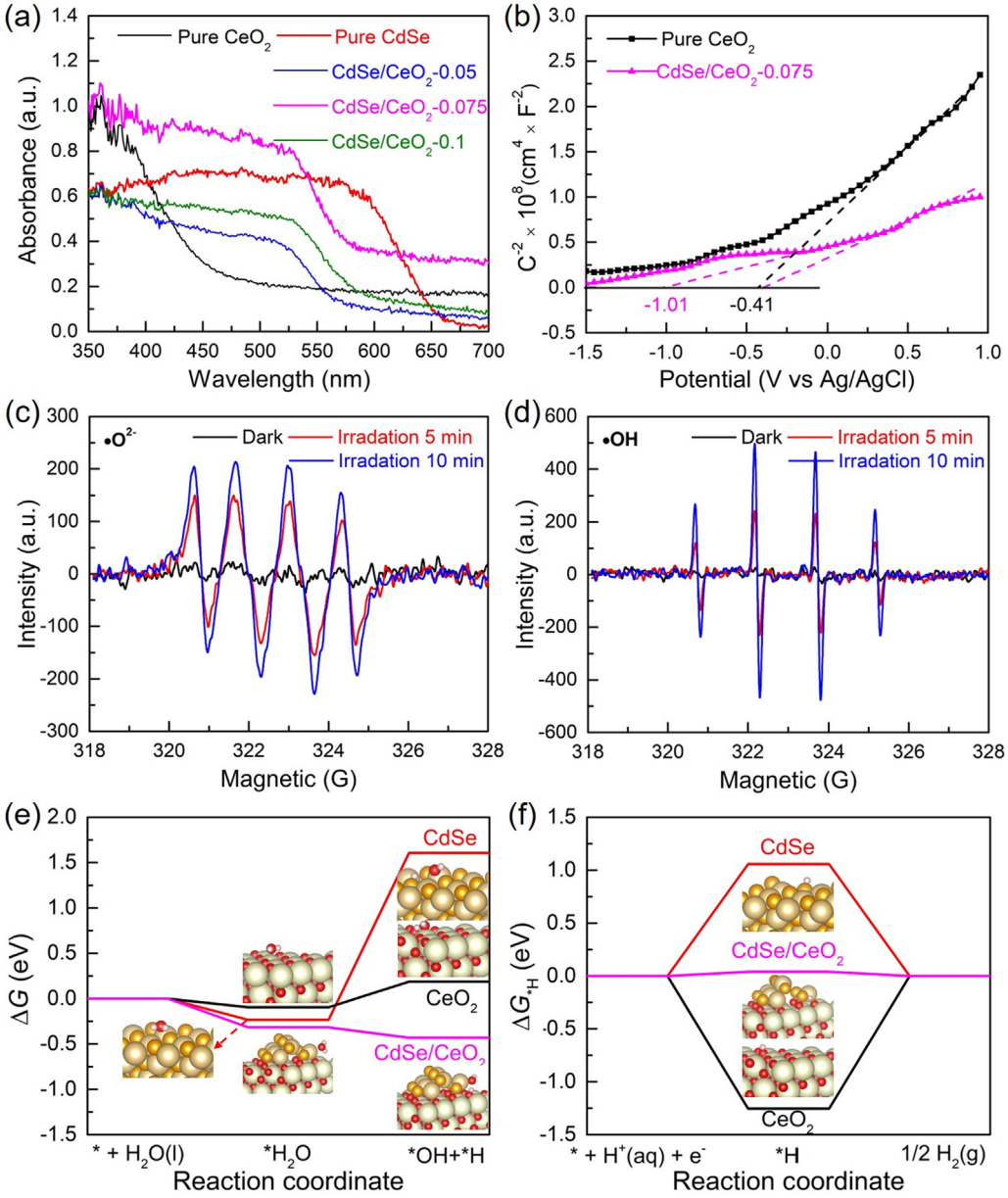

Fig. 4. (a) UV-DRS plots of the as-obtained samples; (b) the MS plots of the CeO_2 and CdSe QDs/CeO_2-0.075 composites; the ESR spectra of CdSe QDs/CeO_2-0.075 composites (c) $\bullet O_2^-$ and (d) •OH under dark and light irradiation. DFT calculated free energy diagram of (e) water adsorption and dissociation and (f) HER on CdSe(1 1 0), CeO_2(1 1 1), and CdSe(1 1 0)/CeO_2(1 1 1).

erated carrier lifetime of CdSe QDs/CeO2-0.075 have been tested by TRPL as shown in Fig. 3 (d). The TRPL of pure CeO_2 and CdSe were shown in Fig. S5 in the Supporting Information. The photogenerated carrier lifetime were 0.5288, 1.99 and 3.2694 ns for pure CeO_2, CdSe and CdSe QDs/CeO_2-0.075, respectively. The increased lifetime of photogenerated carriers of CeO_2 after coating the CdSe QDs is attributed to the fast separation of photogenerated carriers on CdSe QDs and CeO_2 interface[34], that is, the interfacial charge transfer and the improved separation efficiency of photogenerated charge carriers in CdSe QDs/CeO_2 (1 1 1) nanorods could remarkably facilitate the highly efficient photocatalytic HER.

In addition, the UV-diffuse reflectance spectroscopy (DRS) was carried out to inspect the optical absorption properties of CeO_2, CdSe and CdSe QDs/CeO_2 composites, as shown in Fig. 4 (a). From the patterns, it can be found that pure CeO_2 and CdSe exhibit visible-light response at ~ 475 and ~ 655 nm, respectively. For the CdSe QDs-decorated CeO_2 composites, all samples showed improved response in the visible-light region. The higher amount of CdSe QDs in the CdSe QDs/CeO2 composites, the stronger absorption in the visible-light range. The band gaps of the CeO_2 and CdSe are 2.92 eV and 1.95 eV, as shown in Fig. S4 in the Supporting Information. The band gap of pure CdSe in CdSe QDs/CeO_2-0.05, CdSe QDs/CeO_2-0.075, CdSe QDs/CeO_2-0.1 are 2.22 eV, 2.17 eV, and 2.15 eV, respectively. Interestingly, the band gap of CdSe QDs/CeO_2 composites approaches to that of pure CdSe with increased amount of CdSe. Fig. 4 (b) presented the Mott-Schottky (MS) plots of the pure CeO_2 and CdSe, which showed the −0.41 V and −1.01 V vs. Ag/AgCl for the conduction band of CeO_2 and CdSe. They correspond to −0.21 V and −0.81 V vs. NHE of the Fermi band, respectively. Accordingly, ESR (Electron Spin Resonance), was introduced to explore $\bullet O_2^-$ and •OH generated by CdSe/CeO_2 heterostructure as shown in Fig. 4 (c) and (d). No signals were detected for CdSe/CeO_2-0.075 when it was dark. On the contrary, the characteristic signals could be clearly observed under light

irradiation, whose intensity of signals were strengthened with increasing light irradiation time. Therefore, the •OH radicals and $\bullet O_2^-$ radicals were generated for CdSe/CeO_2 heterostructure in the photocatalytic process. The photogenerated electrons and the absorbed O_2 generated $O_2^-\bullet$ and photogenerated holes and the H_2O or OH^- ions generated •OH radicals in the photocatalytic process under light irradiation. Therefore, the possible photocatalytic mechanism is the Z-scheme over the CdSe/CeO_2 heterostructure, see Fig. S6 in the Supporting Information. [35]

To further elucidate the intrinsic reason of enhanced photocatalytic HER activity of the CdSe/CeO_2 photocatalyst, DFT calculations were performed to examine the reactive intermediates and energetics of the key reaction steps on the as-built photocatalyst models (i.e., CdSe(1 1 0), CeO_2(1 1 1), and CdSe(1 1 0)/CeO_2(1 1 1), more details can be found in the Theoretical section in the Supporting Information). For HER in the alkaline electrolyte, the adsorption and dissociation of water are suggested to be one of the potential-determining steps. [36–38] Therefore, the Gibbs free energy profiles regarding the water adsorption and dissociation steps on the CdSe (1 1 0) and CeO_2(1 1 1) surfaces were firstly mapped out, as well as those on the CdSe(1 1 0)/CeO_2 (1 1 1) interface, respectively. For CeO_2 (1 1 1), the most favorable adsorption site is the one above Ce atom, with H atoms in water molecule pointing to O atoms of CeO_2 (1 1 1) surface. Then the water molecular would dissociate to *H and *OH intermediates adsorbed on O and Ce atoms, respectively. However, in the presence of the CdSe/CeO_2 interface, the water molecule would first adsorb at the interface where CeO_2 acts as a water dissociation promoter to produce hydroxyl intermediate which then adsorbs on the nearby CdSe. As shown in Fig. 4 (e), the energy barrier for water dissociation is significantly decreased on the CdSe/CeO_2 interface, and subsequently render this process exothermic, which significantly advance the water dissociation and therefore promotes the *H formation rate. [39] Moreover, we found that the calculated binding energies of H_2O on CdSe, CeO_2, and CdSe/CeO_2 are 0.63, 0.49, and 0.71 eV, respectively. Obviously, the adsorption of water molecules on the CdSe/CeO_2 interface is more energetically favorable and thus further enables the following reactions. With a further analysis of electronic structure, it is suggested that the enhanced water adsorption and lowered energy barrier of water dissociation are attributed to a redistribution of electron density on the CdSe/CeO_2 interface. The Bader charge analysis[40–42] reveals that the electrons are transferred from CdSe to CeO_2 with each Cd atom in CdSe donates 0.1 e to CeO_2 approximately. Consequently, the positive charges around Cd sites strongly help to immobilize H_2O, OH^- and associated intermediates.

For the subsequent reaction step of H* conversion into H_2, a thermo-neutral ΔG_{*H} value of 0 eV is suggested to be desirable by Nørskov and co-workers [43], which correlates with a balance between the rate of proton reduction and the ease of proton removal from the catalyst surface. The *H desorption and H_2 generation would be hindered on the CeO_2(1 1 1) surface due to a strong interaction with *H ($\Delta G_{*H} = -1.25$ eV). In contrast, as shown in Fig. 4 (f), the CdSe/CeO_2 heterostructure yields a ΔG_{*H} of 0.04 eV, being much closer to zero and thus obviously more desirable. Overall, the superior HER catalytic activity of the CdSe/CeO_2 photocatalyst is ascribed to the lowered energy barrier of water dissociation and a thermo-neutral ΔG_{*H} of only 0.04 eV.

3. Conclusions

In summary, the Z-scheme CdSe/CeO_2(1 1 1) heterostructures were successfully constructed by depositing CdSe QDs onto CeO_2 nanorods with exposed (1 1 1) facets. The interface engineering adopted herein not only resulted in the efficient separation of photogenerated carriers but also contributed to the suppressed self-oxidation of CdSe. Furthermore, the DFT calculation results reveal that the CdSe(1 1 0)/CeO_2(1 1 1) interface would enhance the HER activity in the alkaline solution, where CeO_2 promotes water dissociation and CdSe QDs efficiently convert H^+ to H_2. This approach has given a much deeper recognition on heterostructure and uncovered a brand-new gate to increase the efficiency of photocatalytic systems.

Declaration of Competing Interest

The authors declare that they have no known competing financial interests or personal relationships that could have appeared to influence the work reported in this paper.

Acknowledgments

The work is supported by the National Natural Science Foundation of China (11674398), the Fundamental Research Funds for the Central Universities of Central South University (2018zzts016). P.O and J.S thank NSERC Discovery grant (grant # RGPIN-2017-05187), NSERC Strategic grant (grant # STPGP 494012-16), and the Supercomputer Consortium Laval UQAM McGill and Eastern Quebec.

Appendix A. Supplementary data

Supplementary data to this article can be found online at https://doi.org/10.1016/j.jcis.2020.06.100.

References

[1] M.G. Kibria, F.A. Chowdhury, S. Zhao, B. AlOtaibi, M.L. Trudeau, H. Guo, Z.T. Mi, Nat. Commun. 6 (2015) 6797.
[2] A. Q. Zhu, L. L. Qiao, P. F. Tan, Y. J. Ma, W. X. Zeng, R.; Dong and J. Pan, Appl. Catal. B. Environ., 2019, 254, 601–611.
[3] W. Li, X.L. Feng, Z. Zhang, X. Jin, D.P. Liu, Y. Zhang, Adv. Funct. Mater. 28 (2018) 1802559.
[4] Y.Z. Zhang, J. Du, R.C. Luo, Z.Q. Wang, Z.L. Wang, J.H. Han, P. Liu, T. Fujit, Q.K. Xue, M.W. Chen, Nano Energy 58 (2019) 552–559.
[5] F.A. Chowdhury, M.L. Trudeau, H. Guo, Z.T. Mi, Nat. Commun. 9 (2018) 1707.
[6] W.X. Zeng, Y. Bian, S. Cao, Y.J. Ma, Y. Liu, A.Q. Zhu, P.F. Tan, J. Pan, A.C.S. Appl, Mater. Inter. 10 (2018) 21328–21334.
[7] J. Li S.Y. Song Y. Long L.L. Wu X. Wang Y. Xing R.C. Jin X, G. Liu and H. J. Zhang, Adv. Mater. 30 2018 1704416
[8] X.J. Wen, C.G. Niu, L. Zhang, C. Liang, G.M. Zeng, Appl. Catal. B. Environ. 221 (2018) 701–714.
[9] Y.H. Chiu, S.B. Naghadeh, S.A. Lindley, T.H. Lai, M.Y. Kuo, K.D. Chang, J.Z. Zhang, Y.J. Hsu, Nano Energy 62 (2019) 289–298.
[10] S. Chu, P.F. Ou, P. Ghamari, S. Vanka, B.W. Zhou, I. Shih, J. Song, Z.T. Mi, J. Am. Chem. Soc. 140 (2018) 7869–7877.
[11] D.D. Ma, D.K. Sun, Y.J. Zou, S.M. Mao, Y.X. Lv, Y. Wang, J. Li, J.W. Shi, J. Col. Inter. Sci. 549 (2019) 179–188.
[12] J. L. Fu, Q. Q. Yue, H. Z. Guo, C. J. Ma, Y. Y. Wen, H. Zhang, N. W. Zhang, Y. P. Zheng, J. B. Zheng and B. H. Chen, ACS Catal., 2018, 8, 4980–4985.
[13] Q.G. Dai, J.Y. Wu, W. Deng, J.S. Hu, Q.Q. Wu, L.M. Guo, W. Sun, W.C. Zhan, X.Y. Wang, Appl. Catal. B. Environ. 249 (2019) 9–18.
[14] H.W. Du, Y. Wang, H. Arandiyan, J. Scott, T. Wan, D.W. Chu, Catal. Sci. Technol. 8 (2018) 134.
[15] X.L. Yan, T. Hu, P. Liu, S. Li, B.R. Zhao, Q. Zhang, W.Y. Jiao, S. Chen, P.F. Wang, J.J. Lu, L.M. Fan, X.N. Deng, Y.X. Pan, Appl. Catal. B. Environ. 246 (2019) 221–231.
[16] X.P. Fu, L.W. Guo, W.W. Wang, C. Ma, C.J. Jia, K. Wu, R. Si, L.D. Sun, C.H. Yan, J. Am. Chem. Soc. 141 (2019) 4613–4623.
[17] F.Y. Hu, Y. Peng, J.J. Chen, S. Liu, H. Song, J.H. Li, Appl. Catal. B. Environ. 240 (2019) 329–336.
[18] H.W. Ha, S.Y. Yoon, K.J. An, H.Y. Kim, ACS Catal. 8 (2018) 11491–11501.
[19] Y.Q. Su, J.X. Liu, I.A.W. Filot, L. Zhang, E.J.M. Hensen, ACS Catal. 8 (2018) 6552–6559.
[20] X.D. Hao, A. Yoko, C.L. Chen, K. Inoue, M. Saito, G.Y. Seong, S. Takami, T. Adschiri, Y. Ikuhara, Small 14 (2018) 1802915.
[21] G. Spezzati, A.D. Benavidez, A.T. DeLaRiva, Y.Y. Su, J.P. Hofmann, S. Asahina, E.J. Olivier, J.H. Neethling, J.T. Miller, A.K. Datye, E.J.M. Hensen, Appl. Catal. B. Environ. 243 (2019) 36–46.
[22] R. Zhang, X. Ren, S. Hao, R. Ge, Z. Liu, A.M. Asiri, L. Chen, Q. Zhang, X. Sun, J. Mater. Chem. A. 6 (2018) 1985–1990.
[23] Z. Wang, H.T. Du, Z. Liu, H. Wang, A.M. Asiri, X. Sun, Nanoscale 10 (2018) 2213–2217.
[24] Y.J. Ma, J. Jiang, A.Q. Zhu, P.F. Tan, Y. Bian, W.X. Zeng, H. Cui, J. Pan, Inorg. Chem. Front. 5 (2018) 2579–2586.

[25] J.C. Qian, Z.G. Chen, H. Sun, F. Chen, X. Xu, Z.Y. Wu, P. Li, W.J. Ge, A.C.S. Sustain, Chem. Eng. 6 (2018) 9691–9698.
[26] J.C. Qian, Z.G. Chen, F. Chen, Y.P. Wang, Z.Y. Wu, W.Y. Zhang, Z.Y. Wu, P. Li, Inorg. Chem. 57 (2018) 14532–14541.
[27] Y.L. Liu, P.F. Zhang, J.M. Liu, T. Wang, Q.S. Huo, L. Yang, L. Sun, Z.A. Qiao, S. Dai, Chem. Mater. 30 (2018) 8579–8586.
[28] J. Pan, L.L. Zhang, S.T. Zhang, Z. Shi, X. Wang, S.Y. Song, H.J. Zhang, ACS Appl. Nano Mater. 2 (2019) 1516–1524.
[29] P. Wang, X. Li, J.L. Fang, D.Z. Li, J. Chen, X.Y. Zhang, Y. Shao, Y.H. He, Appl. Catal. B. Environ. 181 (2016) 838–847.
[30] Y.Y. Zhong, Y.L. Shao, F.K. Ma, Y.Z. Wu, B.B. Huang, X.P. Hao, Nano Energy 31 (2017) 84–89.
[31] P. Meng, M. Wang, Y. Yang, S. Zhang, L.C. Sun, J. Mater. Chem. A. 3 (2015) 18852–18859.
[32] M. Abdellah, S.H. Zhang, M. Wang, L. Hammarström, ACS Energy Lett. 2 (2017) 2576–2580.
[33] J. W, Shi, D. k. Sun, Y. j. Zou, D. D, Ma, C. He, X. Ji and C. M. Niu, Chem. Eng. J., 2019, 364, 11-19.
[34] Y.J. Ma, Y. Bian, Y. Liu, A.Q. Zhu, H. Wu, H. Cui, D.W. Chu, J. Pan, ACS Sustainable Chem. Eng. 6 (2018) 2552–2562.
[35] R. Subbaraman, D. Tripkovic, D. Strmcnik, K.C. Chang, M. Uchimura, A.P. Paulikas, V. Stamenkovic, N.M. Markovic, Science 334 (2011) 1256–1260.
[36] J. Durst, A. Siebel, C. Simon, F. Hasche, J. Herranz, H. Gasteiger, Energy Environ. Sci. 7 (2014) 2255–2260.
[37] P. Wang, X. Zhang, J. Zhang, S. Wan, S. Guo, G. Lu, J. Yao, X. Huang, Nat. commun. 8 (2017) 14580.
[38] Z. Weng, W. Liu, L.C. Yin, R. Fang, M. Li, E.I. Altman, Q. Fan, F. Li, H.M. Cheng, H. Wang, Nano Lett. 15 (2015) 7704–7710.
[39] G. Henkelman, A. Arnaldsson, H. Jónsson, Science 36 (2006) 354–360.
[40] E. Sanville, S.D. Kenny, R. Smith, G. Henkelman, J. Comp. Chem. 28 (2007) 899–908.
[41] W. Tang, E. Sanville, G. Henkelman, J. Phys.: Conden. Matt. 21 (2009) 084204.
[42] M. Yu, D.R. Trinkle, J. Chem. Phys. 134 (2011) 064111.
[43] J.K. Nørskov, T. Bligaard, A. Logadottir, J. Kitchin, J.G. Chen, S. Pandelov, U. Stimming, J. Electrochem. Soc. 152 (2005) J23–J26.